Monte Carlo simulations of colloidal dispersions under shear

N. Olivi-Tran and R. Botet
Laboratoire de Physique des Solides, Université de Paris–Sud, Bâtiment 510, Centre d'Orsay, 91405 Orsay Cedex, France

B. Cabane
Equipe Mixte, Commissariat à l'Energie Atomique, Rhône-Poulenc, 93308 Aubervilliers, France
(Received 22 July 1997)

We have used a two-dimensional Monte Carlo method to represent the evolution of a colloidal dispersion under shear. This method involves the action of the Derjaquin-Landau-Verwey-Overbeek potential between particles and the action of Brownian motion. The parameters of our simulations have been adjusted to fit the experimental data: temperature and shear velocity. For low volume fractions we find the Newtonian regime where the dispersion evolves as a fluid. For large volume fractions the dispersion has no longer the properties of a fluid. As found experimentally, we observe that it forms a slip layer where only a few particles are located and that allows the dispersion to slip as a whole. [S1063-651X(98)09302-7]

PACS number(s): 47.50.+d, 47.20.−k, 83.20.Jp, 82.70.Dd

I. INTRODUCTION

A colloidal dispersion can be considered as a mixture in which the particles of one component are much larger than those of all the others. If the size difference is sufficiently large, the smaller component can be thought of as forming a fluid that occupies the space between the big particles. Brownian motions of the bigger particles are induced by the collisions of the smaller with the bigger ones.

Nanometric colloidal dispersions resemble molecular fluids for two reasons. First, the Stokes drag force exerted by the solvent on the particles is negligible. Consequently, the motion of the large particles is determined only by interparticle interactions and by thermal agitation. Second, the solvation of particle surfaces by solvent molecules causes the interparticle interactions to be of order of k_BT at ambient temperature, which is the range for fluid behavior. For similar reasons, colloidal dispersions are convenient to study experimentally. For instance, the strength and the range of interparticle potential can be varied through modifications of the solvent composition. In addition, the number density of particles can be easily varied while the fluid remains at ambient pressure.

Transitions from fluid behavior to solid behavior have been observed at high number densities of particles. Fluids that are in the transition region flow in a bizarre way [1]. Typical results have been obtained with nanometric dispersions of silica in water by Persello *et al.* [1]. For dispersions made at low volume fractions of silica, they found normal fluid behavior at all shear rates. However, dispersions made at high volume fractions were found to resist weak shear stresses, and they yield fracture or slip at sufficiently high stress. It is expected that this crossover from fluid to solid response should occur for most fluids as a function of shear rate, i.e., fluid behavior at low shear rates and solid behavior at high shear rates. However, it is not possible experimentally to cover these ranges of shear rates, as some may by be impossibly high to reach ($>10^3$ s^{-1}) or inconveniently slow to follow ($<10^{-3}s^{-1}$). Numerical simulations do not suffer from this limitation, and this was one of the motivations for the present study. The other motivation was the observation that in such conditions the flow field may become inhomogeneous. Indeed, Persello *et al.* [1] have observed that the crossover to a solidlike response is associated with a localization of the shear in a slip layer. Experimentally, it was not possible to determine the composition of the fluid that formed the slip layers, i.e., did it have the same composition as the bulk dispersion or did it have a lower particle concentration. Thus a numerical simulation might be a practical alternative to examine the mechanisms that lead to the formation of slip layers in very concentrated dispersions.

There have been a number of theoretical [2] and computational [3,4] investigations of the effect of high shear rate, though mostly for atomic fluids. Nozieres and Quemada [5] developed a theory to explain the plug formation in shear flow by introducing a lift force that leads the particles to the regions of lower shear. More recently, Schmitt *et al.* [6] wrote a theory based on the coupling between flow and concentration to explain the nonlinear response to shear in such dispersions. From the numerical point of view, Louge [7] used granular dynamics simulations and obtained a phase separation for high shear rates. However, his study failed to explain the real causes of this phase separation. Xue and Grest [8] observed a shear-induced alignment of colloidal particles in a Brownian-dynamics simulation carried out in the presence of an oscillating shear flow.

Monte Carlo simulations are often used in the representation of molecular fluids [9], but they seldom represent the flow of colloidal particles due to the different nature of the interactions between particles and molecules. The originality of our modified Monte Carlo method is that it takes account of the interparticle potential and the Brownian motion of the particles. Moreover, the parameters injected in the simulations are calculated to be very close to the experimental ones, feature that makes the results more realistic than previous simulations.

In this paper we will study numerically the shear flow of nanometric spherical dispersions in a two-dimensional Monte Carlo model. In Sec. II we will present the former

experimental results as well as the different physical characteristics of such dispersions. In Sec. III we will explain the Monte Carlo method that has been used and takes account of the pair potential between particles and their Brownian motion. In Sec. IV results will be introduced. Finally, in Sec. V there will be a comparison with experiments and a general discussion of the model and the results. We will conclude in Sec. VI.

II. EXPERIMENTS

The common characteristic of nanometric silica dispersions is their extremely large surface area. Due to this surface area such dispersions can be used for coatings or to promote sol-gel reactions. Strong repulsions between the particle surfaces are needed in order to retain this surface area.

In water, dispersed particles are usually kept apart from each other due to electrostatic repulsions. It has been proved that colloidal dispersions interact by the mean of the Derjaguin-Landau-Vervey-Overbeek (DLVO) potential [10]. This DLVO potential has an attractive van der Waals part, which can be neglected in most cases, and a repulsive part, which can be represented by the Yukawa potential

$$\frac{U(r)}{k_B T} = \frac{Z^2 L_B}{r} \frac{e^{-\kappa(r-2a)}}{(1+\kappa a)^2}, \tag{1}$$

where $Z = 4a/L_B$, a is the particle radius, κ is the screening efficiency, and L_B is the Bjerrum length of water. At contact ($r = 2a$), for $a = 10$ nm, $Z = 60$, and $\kappa^{-1} = 10$ nm the repulsive energy is $30 k_B T$. This energy allows the dispersion to remain stable for long times, for several months.

If the pair interaction energy of particles at a distance r is $U(r)$, then the neighbors of a particle are effectively excluded from a region of radius a_{eff} around it [11]. Experimentally, it has been shown that the range of interactions is a_{eff} is very close to $a + \kappa^{-1}$. Finally, the effective volume fraction ϕ_{eff} used by the particles can be calculated as

$$\phi_{eff} = \phi (a_{eff}/a)^d, \tag{2}$$

where d is the dimension of space.

The response of dispersions to mechanical testing may be of two types: linear viscous response to small stresses and nonlinear response to large stresses that may change the structure of the dispersion [12]. For the colloidal dispersions studied experimentally and numerically here, the occurrence of either behavior is determined by the volume fraction. For low volume fraction, we recovered the gaslike state: Linear response was found in all cases unless the shear rate exceeds the rates of spontaneous (Brownian) motion for individual particles that are on the order of 0.4 $\mathrm{m\,s^{-1}}$. For large volume fraction, i.e., for $\phi_{eff} > 1$, the dispersions have the appearance and general properties of physical gels without having their connectivity. They may be defined as soft solids.

Rheological experiments at a steady state were performed on the silica dispersions [1]. To compare the shear rate to the Brownian velocity, it is important to introduce the Péclet number

$$\mathrm{Pe} = \frac{a^2 \dot{\gamma}}{D_0}, \tag{3}$$

where a is the particle radius (10^{-8} m), D_0 the self-diffusion coefficient of isolated particle in water (2.45×10^{-11} $\mathrm{m^2\,s^{-1}}$), and $\dot{\gamma}$ the shear rate. In these experiments, the Péclet number was always low ($\mathrm{Pe} = 10^{-2}$).

For samples made in the gaslike state at very low volume fractions ($\phi_{eff} \ll 1$), the stress induced by the shear rate was relaxed quasi-instantaneously. In fact, the shear rate was kept low enough so that spontaneous relaxations of the dispersion kept it near equilibrium while it was perturbed. An experimental criterion for this regime was a measured stress proportional to the shear rate (Newtonian behavior).

For dispersions in the soft solid state, at the applied shear rates (from 8×10^{-4} to 0.8 $\mathrm{s^{-1}}$). the lack of free volume ($\phi_{eff} > 1$) quenches the spontaneous motion, which would restore equilibrium. It was found that the stress remains on a plateau, independent of shear rate, over nearly five decades in shear rates. The bulk of the sample remained undeformed while all the shear was concentrated in a small layer either in the bulk itself (internal slip) or near the wall (wall slip). This fracture allowed the stress to remain on a plateau.

III. MODEL

We use a Monte Carlo method modified to take account of the Brownian motion of the particles and of the potential created by the electrostatic repulsions between the particles. The circular particles are moving on a two-dimensional triangular lattice [see Fig. 1(a)]. In order to remove finite-size effects, we impose periodic boundary conditions on the left- and right-hand sides of the simulation box. The bottom limit is static and the upper limit has a nonzero velocity. To simplify the impulsion transmission from the two limiting walls, we have simply stick particles on them, each of these particles having the velocity of its corresponding wall. The positions of the particles are limited to the lattice intersections, as in the lattice-gas model.

At the beginning of the simulation, the particles have only a Brownian velocity: The additional velocity imposed by the moving wall is transmitted to them during the whole simulation. At each Monte Carlo step (MCS), one particle is chosen with a probability proportional to its velocity; this allows one to obtain a MCS that is similar to a time scale. To determine the motion direction, the velocity vector is projected on the grid and the direction is chosen with a probability proportional to the projections [see Fig. 1(b)]. Then this particle interacts with its nearest neighbor in the direction of its projected motion. Afterward, the chosen particle is moved on the lattice along its new velocity direction: At best, it moves to the very next site with respect of its velocity direction if there is no particle on this neighboring site.

An important feature of this simulation is that the particles interact through the Yukawa potential. This potential acts on two levels: first, on the particle motion and second, on the direct interaction between two particles. Indeed, one particle can move itself only when the potential gradient in the direction of its motion is negative or if its kinetic energy allows it to overcome the potential barrier.

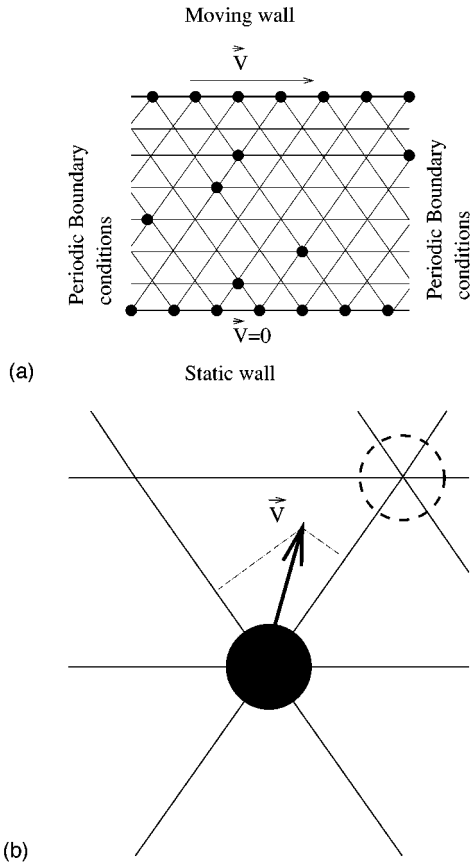

FIG. 1. (a) Representation of the simulation box, which has periodic boundary conditions on the left- and right-hand sides. The box is limited on the top by a moving wall with constant velocity and is limited on the bottom by a static wall. The particles are, at the beginning of the simulation, put at random on the triangular lattice. In order to simplify the impulsion transmission from the two walls, particles have been stuck on them. (b) The velocity of each particle is computed off lattice, but the motion of the particle are on lattice. In addition, the particle positions remain on the intersections of the grid. The arrow represents the velocity vector before displacement and the dashed circle represents the most probable position of the particle after motion.

The direct interaction of two particles is computed by a classical mechanics equation [13]

$$\alpha=\int_{r_{min}}^{\infty}\frac{\rho\dfrac{dr}{r^2}}{\sqrt{1-\dfrac{\rho^2}{r^2}-\dfrac{2U}{mv_\infty^2}}}, \tag{4}$$

where U is the Yukawa potential, ρ is the impact parameter, and v is the reduced velocity (velocity of the center of mass of the two particles) before the interaction and if one considers that they come from infinity, r_{min} is the square root of the integrand. So the deviation angle χ for the trajectory of the reduced particle is

$$\chi=|\pi-2\alpha|. \tag{5}$$

Then it is easy to compute the real deviation and velocities of the two particles 1 and 2 knowing that their position vectors are related to the position vector of the reduced particle by $\vec{r}=\vec{r}_1-\vec{r}_2$. So the interaction between two particles is elastic.

The Yukawa potential depends on the temperature T [see Eq. (1)]; so it is essential to calculate k_BT in our Monte Carlo system. The temperature of the dispersion is closely related to the Brownian-motion velocity. The classical Langevin equation is

$$\dot{p}_i(t)=-\xi p_i(t)+\tilde{p}_i(t), \tag{6}$$

where ξ is the friction constant, p_i is the momentum of a single particle i, and $\tilde{p}_i$ is the random force. This random force acts on the particles and induces a random motion. In our simulation, we have simply computed this random motion by adding at each Monte Carlo step a random velocity. The random velocity distribution is a Gaussian and in our case $\langle\vec{v}^2\rangle=1$. The autocorrelation function of this random force is given by

$$\langle\tilde{p}_i(t)\tilde{p}_i(0)\rangle=2mk_BT\xi\delta(t). \tag{7}$$

At long times, particles motions generated by Eq. (6) conform to Einstein's relation

$$2tD=\frac{1}{3}\langle|\vec{r}_i(t)-\vec{r}_i(0)|^2\rangle, \tag{8}$$

with ξ related to the diffusion coefficient D by

$$\xi=k_BT/mD. \tag{9}$$

We do not know the diffusion coefficient D, but the friction constant ξ can be approximated knowing the Stokes drag force

$$\vec{F}_{drag}=-8\pi a\eta\vec{v}=m\frac{d\vec{v}}{dt}, \tag{10}$$

where a is the particle radius and η is the viscosity of the surrounding fluid. The breaking action of the surrounding fluid has been represented via this Stokes drag force. To compute the time, we need a characteristic velocity and a characteristic length in the simulation. We have chosen v_{wall}, which is the velocity of the moving wall, as the characteristic velocity and the diameter of the particles $2a$ as the characteristic length. So, by approximating the time dt by $2a/v_{wall}$, we obtain

$$\xi\propto\frac{32\pi a^2\eta}{mv_{wall}}. \tag{11}$$

Conversely, the Brownian velocity is related to the temperature T by the well-known relation

$$\langle v^2\rangle=k_BT/m. \tag{12}$$

Thus writing $s^2=\vec{v}_{wall}^2/\langle\vec{v}^2\rangle$, we obtain

$$k_BT=\frac{1}{m\xi^2s^2}(32\pi a^2\eta)^2, \tag{13}$$

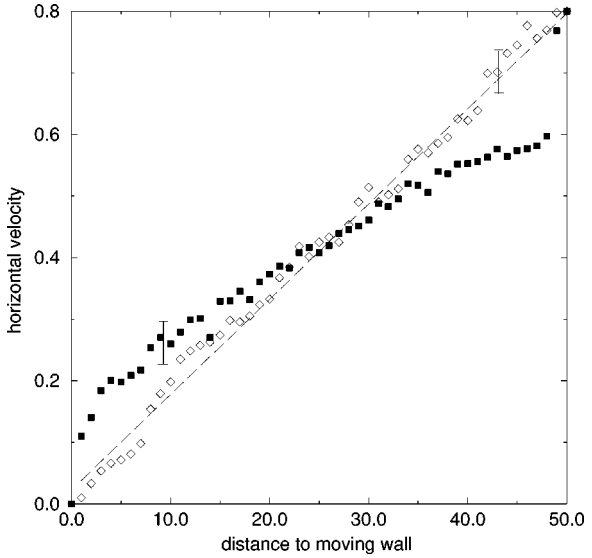

FIG. 2. Horizontal velocity profile ($m\,s^{-1}$) as a function of the distance from the moving wall (in units of 20 nm) for $\phi=0.1$ (white diamonds) and for $\phi=0.5$ (black squares) and $\dot{\gamma}=0.8\ s^{-1}$. The evolution of the velocity is linear on average for the lower surface fraction, which is characteristic of a Newtonian regime in a Couette geometry. For the higher volume fraction, the is a slip near the two walls and the flow is no longer Newtonian.

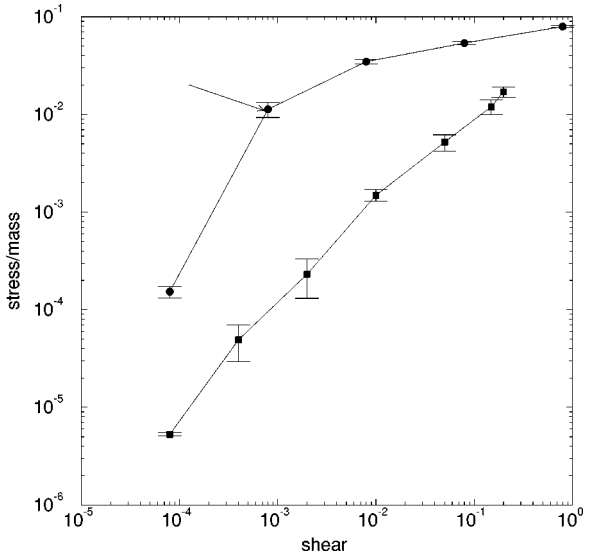

FIG. 3. A log-log plot of the numerical evolution of the non-Brownian stress (N/kg) as a function of the applied shear rate (s^{-1}) within the experimental interval for two surface fractions: $\phi=0.1$ (squares) and $\phi=0.3$ (circles). The stress evolves linearly with the shear rate for the lower concentration (Newtonian regime). For the higher surface fraction, the stress increases and reaches a threshold. The arrow shows the transition location from fluid to soft solid state.

so the Yukawa potential can be computed, taking account of the temperature, the particle radius, and the interparticle distances.

In the following we will present results including the evolution of the stress as a function of the surface fraction. To compute this stress, we have calculated the transfer of the tangential impulse of the particles to the static wall.

IV. RESULTS

Experimentally, the Brownian velocity of the particles is about 0.4 $m\,s^{-1}$ and the shear rate is $(8\times10^{-4})-0.8\ s^{-1}$. We have calculated the parameters $k_BT, U(r)$ of our simulation as a function of the coefficient s, which is the rate between the Brownian velocity and the moving wall velocity, and as a function of the length scale of the lattice ($=20\times10^{-8}$ m). The other parameters such as the friction constant ξ and s have been deduced from experimental data: $\xi=10^{-5}$, $a=10^{-8}$ m, and $\eta=10^{-3}$ Pa s.

We reached the steady state of the flow for about 500 MCS per particle. For low surface fractions (i.e., $\phi=0.1$ and $\phi_{eff}\ll1$) , we recovered a Newtonian flow regime where the horizontal parts of the velocity vectors increase linearly from the static wall to the moving wall. In order to obtain the horizontal velocity profile, we had to average, with respect to the MCS, this velocity profile on the same simulation. In Fig. 2 the black circles represent the velocity profile in the Newtonian regime. The regression on this curve, which is represented by a long-dashed line, shows that the evolution of the velocity is linear in this case. This regime occurs for low surface fractions $\phi<0.3$. On the same figure, we have plotted the horizontal velocity profile (white diamonds) for a higher surface (volume) fraction $\phi=0.5$ ($\phi_{eff}\gg1$). As one can see, there is a steep increase of the velocity near the static wall as well as near the moving wall. The velocity increases more slowly in the bulk of the dispersion. This plot is not symmetric due to the history of the mechanism: At time $t=0$, the dispersion is at rest with respect of the Brownian motion of particles; then when the upper wall begins to move, the particles cannot follow its motion due to the lack of free surface (volume). It is only when the dispersion reaches the steady state that it begins to slip near the static wall. So the difference between the velocity of the wall and the velocity of the dispersion is greater near the moving wall than near the static wall.

In Fig. 3 we show the evolution of the stress (which is calculated by computing the transfer of the tangential impulse to the static wall) with the applied shear rate for two different surface (volume) fractions $\phi_{eff}\ll1$ ($\phi=0.1$) and $\phi_{eff}\gg1$ ($\phi=0.5$). In this case, we have computed only the stress induced by non-Brownian motion; the stress due to the Brownian behavior of particles has been removed. As one can see for the lower surface (volume) fraction, the stress is proportional to the shear rates: This shows that the flow is Newtonian. However, for the higher surface (volume) fraction, we can see that there is a saturation of the stress: The slipping of the dispersion that is a consequence of the high stress allows the resulting stress to become steady regardless of the shear rate.

So there is a transition between the fluid and the soft solid state (see Fig. 4). This transition occurs, in two dimensions, between $\phi=0.2$ ($\phi_{eff}=0.8$) and $\phi=0.3$ ($\phi_{eff}=1.2$) in the limit of the applied shear rates (in this case we chose $\kappa^{-1}=10$ nm). The nonlinear evolution of the horizontal velocity profile has been taken as the characteristic of the soft solid state. Figure 4 can be seen as a phase diagram between the fluid state and the soft solid state. This transition occurs when the free volume, i.e., the volume between the effective

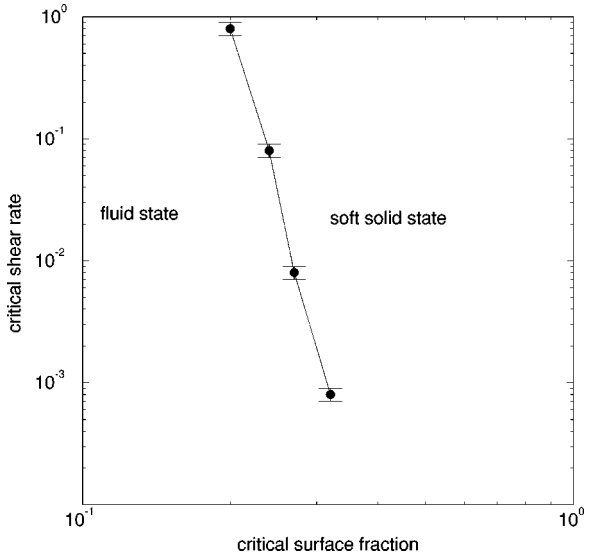

FIG. 4. A log-log plot of the critical applied shear rate (s^{-1}), which corresponds to the fluid to soft solid state transition, versus the surface fraction (dimensionless). The evolution of the critical applied shear rate allows one to obtain a phase diagram on the same figure: There are two regions, Newtonian behavior and soft solid behavior, which depend on the applied shear rate and the surface fraction.

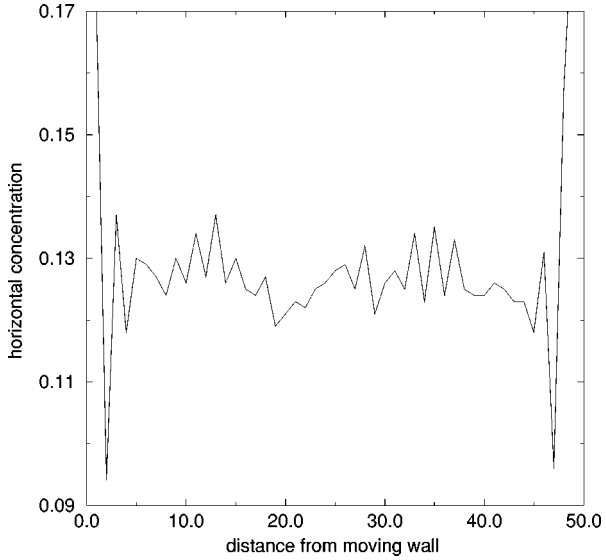

FIG. 5. Horizontal particle concentration (μm^{-1}) versus the distance (in units of 20 nm) to the moving wall ($\phi=0.5$). This concentration decreases at two given points. These points do not have a fixed location: They depend on the simulation, although the same parameters were used.

particles, is close to zero or even when the effective particles overlap. When the free volume decreases, the dispersion cannot release the stress by particles displacement. So the mechanical response to stress may be different from that in the fluid state as one can see in the following. We can see that the end of the Newtonian regime occurs for $\phi=0.2$ ($\phi_{eff}=0.8$).

To see the effect of high stress on the structure of the dispersion, we have also plotted the horizontal particle density as a function of the distance to the moving wall. Obviously, there is a dip of this density at two given distances (Fig. 5). The depth of these dips increases with the applied shear rates. The locations of these dips are not fixed: They change for different simulations with the same applied shear rate and same surface (volume) fraction. Moreover, the number of these layers varies between one and two. To visualize this concentration change, refer to Fig. 6, where a portion of the simulation box has been represented. It is easy to remark that there is a lack of particles on two given horizontal lines in the dispersion. Experimentally, two adhesion conditions have been used: slippery walls where the depleted layer was located near the wall and adhesive walls where the layer was located anywhere in the sample. For the numerical computations, the wall can be thought of as adhesive since we did not add any repulsive potential for the particles sticked on the wall. So the difference of potential between the wall and the bulk is negative and thus can be considered as attractive.

Because the walls induced a break in the continuity of the sample, the slip layer was mostly located near the walls. Over more than 100 simulations, this layer appeared either near the moving wall or near the static wall. This transient lack of particles may be enlarged when stress reaches the threshold . Finally, we have computed the transfer of the normal impulse to the static wall for a surface (volume) fraction $\phi_{eff} \gg 1$. When the shear rate increases from 8×10^{-4} to 0.8 this impulse transfer varies from 10^{-2} to 1.8. We have observed the same phenomenon on the moving wall. This observation is in accordance with the theory of Nozieres and Quemada [5], who intuited a lift force in the dispersion to explain the formation of a plug in the dispersion.

V. DISCUSSION

The central result of this work is the observation of a crossover from fluidlike flow to solidlike slipping in the numerical simulation of a concentrated dispersion. We recover the fluid behavior at low surface (volume) fractions. In the numerical simulations, the fluid behavior is characterized by a horizontal velocity profile that is a linear function of the

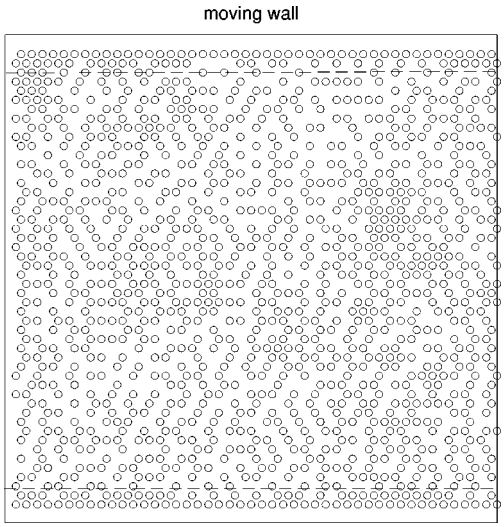

FIG. 6. Example of the simulation box for high surface (volume) fraction ($\phi=0.5$). The dispersion is homogeneous except on two given horizontals (represented by horizontal dashed lines), where there is a lack of particles.

distance to the static wall (Fig. 2). Thus all the horizontal lines of particles are moved at the same shear rate with respect to their neighbors. As a result of this shear, there is a tangential stress exerted on the walls and this stress grows proportionally to the shear rate. Consequently, the fluid is Newtonian at the shear rates used in the simulation. This fluid behavior is explained by the fact that there is sufficient free volume for the particles to move with respect to the applied shear rate. Indeed, for the surface (volume) fractions that show fluid behavior, the range of the potential (screening length κ^{-1}) is small with respect to the interparticle distances. In this case, the effect of the potential on the behavior of the fluid is small; consequently, the method used here to describe the fluid is similar to the classical method introduced by Metropolis *et al.* [9].

At higher surface (volume) fractions, we observe a transition to solidlike slipping. The criterion used to recognize the transition is the observation of a nonlinear velocity profile (Fig. 2). At the same time, we observe two dips in the concentration profile, which mark the locations of the slip layers (Fig. 5). A quantitative determination of the threshold shows that it depends on the shear rate (Fig. 4). Accordingly, there is, for each dispersion, a critical shear rate below which it can accommodate the shear and beyond which it will slip as a solid. This transition may be explained by the fact that the dispersions of higher surface (volume) fractions have little free volume available and therefore shear motion results essentially from the motion of vacancies. Consequently, there is a critical shear rate where it becomes more efficient to concentrate vacancies in one line near the wall rather than distribute them throughout the fluid.

It is interesting to note, however, that the bulk part of the sample continues to deform slowly after the threshold has been reached: Immediately after the motion of the walls was initiated, the velocity profile was flat and then it deformed progressively at long times (Fig. 2 shows the velocity profile at long times). Thus the solid deforms at the maximum rate allowed by the concentration of vacancies and the excess shear rate is taken up by the depleted region.

Three theories have been proposed to explain the formation of one or several depleted layers beyond the transition from fluidlike to solidlike behavior. First, the alignment of planes of particles in the shear has been observed in colloidal crystals made of particles larger than the colloidal silicas studied here [14–18]. Xue and Grest [8] found numerically this alignment, but also for larger particles. Though we have been working on lattice, we did not observe this alignment. Second, there is disorganization of the particles under shear (''melting'') [17,19]. Typically, there is shear alignment at low shear rates and then shear melting at higher shear rates. The stress raises sharply when melting occurs. In this case too we did not observe either the alignment at low shear rates or the stress increase. Finally, the last theory is that any process that increases the amount of free volume in a particular layer will turn this layer into a slip layer. This theory is very close to that of Nozieres and Quemada [5], who proposed the existence of a lift force that could separate the bulk into two parts. It is also close to the calculations of Schmitt *et al.* [6] on the flow-concentration coupling.

Numerically, beyond the transition from fluidlike to solidlike behavior, we observe that the stress remains constant

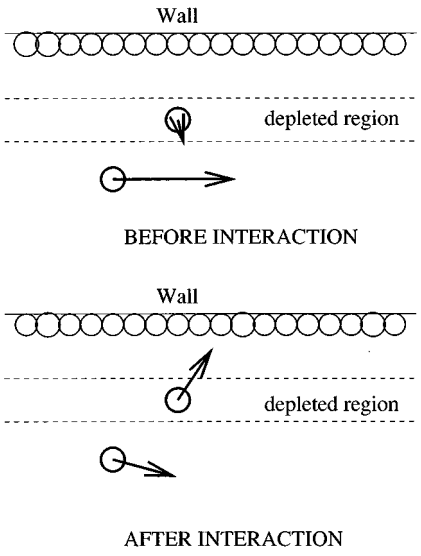

FIG. 7. Behavior of the particles near the slip layer.

regardless of the applied shear rate (Fig. 3). This is indeed the behavior observed in the experiments on the ''real'' dispersions and it corresponds to what is generally called a solidlike slip. Still, we need to explain how the material manages to keep the stress locked at a constant level. The information obtained from the simulation is that the two dips in the concentration profile become deeper still when shear rate is increased beyond the critical shear rate. This obviously explains why the slipping becomes more efficient. However, we can also examine which process in the simulation maintains the dips in the concentration profile. This process may be described as follows. Consider one particle in one of the depleted lines and a neighboring particle in the dense line next to it towards the wall. Due to the high horizontal (due to the shear direction) velocity of the particle in the dense line, a collision between the two particles will more frequently cause the particle in the depleted layer to acquire a velocity that pushes it away from the wall (Fig. 7). Thus it is a simple feature of the elastic interaction that causes one line of particles near the wall to be depleted. Any increase in the velocity of the wall causes a stronger depletion, which allows the stress to remain constant.

In a more quantitative way, we need to explain why there is a threshold for this effect and why the stress remains constant beyond the threshold. The depletion that we observe may be characterized by a ''normal'' force that keeps the particles away from the wall. We have computed this ''lift'' force, as mentioned in the preceding paragraph and found that it increases regularly with the shear. This normal force is opposed by the osmotic pressure of the fluid that tends to fill the depleted layer. Consequently, the threshold for the formation of a depleted layer must be reached when this lift force exceeds the osmotic pressure of the fluid.

On a more global level, this explanation appears to be in line with the theory of Nozieres and Quemada [5], who proposed the existence of a lift force that could separate the bulk fluid into two parts. It is also close to the analysis of Schmitt *et al.* [6], who postulate a flow-concentration coupling to explain these phenomena. The differences with the two other theories [17,19,8] may be explained by the different potential

that has been used here. We may recover other behaviors of the dispersions if we employ, for example, a long-range potential.

VI. CONCLUSION

We have used here a Monte Carlo method that takes account of the Brownian motion of the particles and of the interparticle potential. These additive characteristics of the method have allowed us to recover the phase separation of concentrated colloidal dispersion and gave also a good representation of the fluid state of these dispersions. The numerical parameters are in accordance with the experimental ones (temperature and rate of shear velocity with Brownian velocity), so this method allows one to compare numerical results with experimental ones and may represent the local concentration of particles that cannot be determined experimentally. It is known that, in rheology, dispersion may have two different behaviors: Solidlike and fluidlike. Here we have shown that for given volume fractions, a dispersion may have these two behaviors.

Moreover, we were able to analyze the slip layer which allows the dispersion to lower the stress due to the shear, and we were able to show that the slip layer is in fact a small fluid region, in opposition with the bulk, which is in a soft solid state, a feature that was not possible to determine experimentally.

It might be interesting now to change other parameters and constants in this model such as the monodispersity of the particle by introducing two particle sizes and the shape of the particles (for example, to simulate the rheological properties of plane-shaped particles). Moreover, it would be simple to change the interparticle potential by adding a small van der Waal attractive part.

ACKNOWLEDGMENTS

We would like to thank Bernard Bernu and Luc Belloni for fruitful discussions. This work was supported in part by funds from CNRS DIMAT.

[1] J. Persello, A. Magnin, J. Chang, J. M. Piau, and B. Cabane, J. Rheol. **38**, 1845 (1994).
[2] T. R. Kirkpatrick and J. C. Nieuwoudt, Phys. Rev. Lett. **56**, 885 (1986).
[3] J. J. Erpenbeck, Phys. Rev. Lett. **52**, 1333 (1984).
[4] L. V. Woodcock, Phys. Rev. Lett. **54**, 1513 (1985).
[5] P. Nozieres and D. Quemada, Europhys. Lett. **2**, 129 (1986).
[6] V. Schmitt, C. M. Marques, and F. Lequeux, Phys. Rev. E **52**, 4009 (1995).
[7] M. Y. Louge, Phys. Fluids **6**, 2253 (1994).
[8] W. Xue and G. S. Grest, Phys. Rev. Lett. **64**, 419 (1990).
[9] N. Metropolis, A. W. Rosenbluth, M. N. Rosenbluth, A. H. Teller, and E. Teller, J. Chem. Phys. **21**, 1087 (1953).
[10] J. W. Vervey and J. Th. Overbeek, *Theory of the Stability of Lyophobic Colloids* (Elsevier, Amsterdam, 1948).
[11] J. A. Barker and D. Henderson, J. Chem. Phys. **47**, 2846 (1967).
[12] J. W. Goodwin and R.W. Hughes, Adv. Colloid Interface Sci. **42**, 303 (1992).
[13] L. Landau and E. Lifshitz, *Mécanique* (Editions de la Paix, Moscow, 1980).
[14] M. Tomita and T. G. M. Van de Ven, J. Colloid Interface Sci. **99**, 374 (1984).
[15] B. J. Ackerson, Physica A **174**, 15 (1991).
[16] B. J. Ackerson, J. B. Hayter, N. A. Clark, and L. Cotter, J. Chem. Phys. **84**, 2344 (1986).
[17] H. M. Laun, R. Bung, S. Hess, W. Loose, K. Hahn, E. Hadicke, R. Hingmann, F. Schmidt, and P. Lindner, J. Rheol. **36**, 743 (1992).
[18] L. B. Chen, B. J. Ackerson, and C. F. Zukoski, J. Rheol. **38**, 193 (1994).
[19] H. M. Lindsay and P. M. Chaikin, J. Chem. Phys. **76**, 3774 (1982).